

Cell-Oriented Modeling of *In Vitro* Capillary Development

Roeland M.H. Merks^{1,2}, Stuart A. Newman², and James A. Glazier¹

¹ Biocomplexity Institute
Department of Physics
Indiana University
Bloomington, IN 47405

post@roelandmerks.nl, glazier@indiana.edu
<http://biocomplexity.indiana.edu>

² Cell Biology and Anatomy
New York Medical College
Valhalla, NY

newman@nyc.edu
<http://www.nyc.edu/sanewman>

Abstract. We introduce a Cellular Potts model (a cellular-automaton-based Monte-Carlo model) of *in vitro* capillary development, or angiogenesis. Our model derives from a recent continuum model, which assumes that vascular endothelial cells chemotactically attract each other. Our discrete model is “cell based.” Modeling the cells individually allows us to assign different physicochemical properties to each cell and to study how these properties affect the vascular pattern. Using the model, we assess the roles of intercellular adhesion, cell shape and chemoattractant saturation in *in vitro* capillary development. We discuss how our computational model can serve as a tool for experimental biologists to “pre-test” hypotheses and to suggest new experiments.

1 Introduction

A detailed understanding of capillary blood vessel formation, or angiogenesis, is essential to understand and control physiological and pathological processes from wound healing to tumor growth and angiogenesis-related pathologies such as advanced diabetic nephropathy. Capillaries develop in two main ways: through the aggregation of endothelial cells into capillary cords, and through sprouting from existing capillaries.

In vitro culture of human umbilical vascular endothelial cells (HUVEC) in Matrigel is a popular experimental model of capillary development (see *e.g.* [2]). Matrigel is an extracellular matrix product obtained from murine tumors. The extracellular proteins and growth factors in the gel stimulate HUVEC cells to form networks (Fig. 1) resembling vascular networks *in vivo*. HUVEC-Matrigel cultures and related HUVEC cultures in collagen [3] and fibrin [4] gels are standard models in biomedical research to identify the key molecular players in

pathological and physiological angiogenesis, to unravel the role of cell growth and apoptosis in vasculogenesis and to probe potential anti-angiogenic pharmaceuticals.

The biophysical mechanisms by which endothelial cells form such networks are poorly understood. Several computational studies have suggested that endothelial cells, behaving according to a small set of rules, could suffice to explain network-formation. Most hypotheses assume that either chemotaxis [5,6] or tractional forces relayed through the extracellular matrix [4,7,8] drive cell aggregation. Partial differential equation models of both mechanisms generate patterns that resemble *in vitro* networks, so which of them most closely parallels the biological mechanism remains unclear.

These continuum approaches implicitly assume that the endothelial cells that construct the pattern are much smaller than the length-scale of interest, namely that of the “cords” and “nodes.” *In vitro*, however, at most a dozen elongating cells form the cords, which are one to a few cell-diameters thick (see Fig. 1). Thus, we expect the scale of the endothelial cells to play an important role in patterning. The properties of individual cells, such as their shape, their mutual adhesion and their adhesion to the extracellular matrix may also affect the pattern resulting from their interaction.

This paper develops a *cell-oriented* approach to modeling *in vitro* vasculogenesis, based on the Gamba-Serini chemotaxis model [5,6]. We construct computational models of individual HUVEC cells which mimic experimentally-observed cell phenomenology, including response to external chemical signals, cell elongation, cell adhesion, chemotaxis, haptotaxis, *etc.* We then release these simulated cells in a “virtual Petri-dish” and quantitatively compare their macroscopic, collective behavior to experiments. We attempt to recover minimal sets of physicochemical properties and behavioral rules for the cells which reproduce the experimentally-observed tissue-level pattern.

Our focus on cell phenomenology may seem crude compared to large-scale, post-genomic, systems-biology initiatives whose aim is to model *ab initio* and in detail the internal structure and genetic regulation of individual cells, and even-

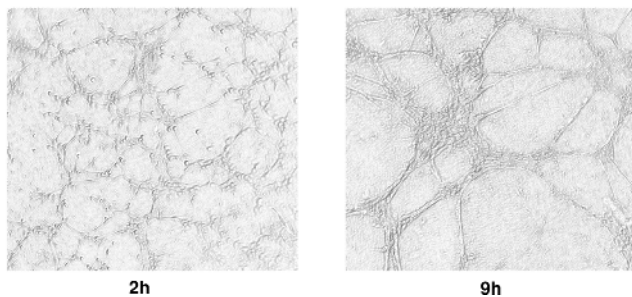


Fig. 1. HUVEC culture on Matrigel, 4x magnification, 2h (left) and 9h (right). To improve contrast, we have applied an Opening Top-Hat transform [1] with a small-disk structuring element.

tually collections of interacting cells (see *e.g.* [9,10]). However, the cell-oriented approach allows us to distinguish a) how genomic information determines cell phenomenology (using detailed, single cell models) from b) how collections of cells exhibiting a particular phenomenology interact during biological morphogenesis (using a “cell-oriented” approach). The cell-oriented approach has been successful in the study of biological morphogenesis. In particular, it can simulate the entire developmental life cycle of the cellular slime mold *Dictyostelium discoideum* [11,12], convergent extension in early vertebrate embryos [13], tumor invasion [14] and pattern formation in vertebrate limb cell cultures [15].

The Cellular Potts model (CPM) [16,17], a cellular-automaton-based Monte-Carlo method, is a convenient cell-oriented simulation framework. Early CPM studies of differential-adhesion-driven cell rearrangement in cell aggregates quantitatively reproduced cell sorting experiments [16]. An energy-minimization philosophy, a set of energy constraints and auxiliary conditions determine how cells move. Connections between cells determine a cell-cell contact (or bond) energy, favoring stronger over weaker bonds and shortening of the boundary length. An energy constraint regulates cell volume or area. Further constraints or auxiliary conditions easily extend the CPM to include chemotaxis [11], cell growth, cell death [18] and cell polarity [13].

The remainder of this paper introduces our hybrid CPM/PDE model and extensions to the CPM motivated by HUVEC phenomenology. We then study patterning in the CPM/PDE version of the Gamba-Serini chemotaxis model. Finally, we discuss the biological and computational relevance of our results.

2 Methods

2.1 Hybrid Cellular Potts Model

We use a hybrid Cellular Potts (CPM) and partial differential equation (PDE) model (see [11,12,17]). The CPM models endothelial cells, while the PDEs model the chemoattractant. Experimentally-confirmed cell behaviors, which we include in the model are, 1) secretion of chemoattractants, 2) chemotaxis of cells up chemical gradients, and 3) progressive elongation of cells.

The CPM represents biological cells as patches of lattice sites, \mathbf{x} , with identical indices $\sigma(\mathbf{x})$, where each index identifies, or “labels” a single biological cell. Connections between neighboring lattice sites of unlike index $\sigma(\mathbf{x}) \neq \sigma(\mathbf{x}')$ represent membrane bonds, with a characteristic *bond energy* $J_{\sigma_{\mathbf{x}},\sigma_{\mathbf{x}'}}$, where we assume that the types and numbers of “cell adhesion molecules” (CAMs) of the interacting cells determine J . An energy penalty increasing with the cell’s deviation from a designated target volume A_{σ} imposes a *volume constraint* on the biological cells. To mimic cytoskeletally driven membrane fluctuations, we randomly choose a lattice site, \mathbf{x} , and attempt to copy its index $\sigma_{\mathbf{x}}$ into a randomly chosen neighboring lattice site \mathbf{x}' . To ensure isotropy, we use the twenty, first- to fourth-order neighbours on a square lattice. On average, we attempt an update at each lattice site once per Monte-Carlo step (MCS). We calculate how much

the Hamiltonian would change if we performed the copy, and accept the attempt with probability:

$$P(\Delta H) = \{\exp(-(\Delta H + H_0)/T), \Delta H \geq -H_0; 1, \Delta H < -H_0\}, \quad (1)$$

where $H_0 > 0$ is an energy threshold which models viscous dissipation and energy loss during bond breakage and formation [18]. We then define the Hamiltonian as:

$$H = \sum_{\mathbf{x}, \mathbf{x}'} J_{\sigma_{\mathbf{x}}, \sigma_{\mathbf{x}'}} (1 - \delta_{\sigma_{\mathbf{x}}, \sigma_{\mathbf{x}'}}) + \lambda \sum_{\sigma} (a_{\sigma} - A_{\sigma})^2, \quad (2)$$

where λ represents resistance to compression, and the Kronecker delta is $\delta_{x,y} = \{1, x = y; 0, x \neq y\}$. The cells reside in a “medium” which is a generalized CPM cell without a volume constraint and with $\sigma = 0$. In most simulations, we use a bond energy $J_{cc} = 5$ between the endothelial cells, and $J_{cM} = 20$ between the endothelial cells and the medium. We further define a *surface tension* $\gamma_{cM} = J_{cM} - J_{cc}/2$, which enables us to determine whether the cells cohere ($\gamma_{cM} > 0$) or dissociate ($\gamma_{cM} < 0$) [16] in the absence of chemotaxis. Our default cellular adhesion setting is adhesive, *i.e.* $\gamma_{cM} > 0$. We define a special, high *cell-border energy* $J_{cB} = 100$ to prevent cells from adhering to the boundaries. The viscous dissipation H_0 and all terms in the Hamiltonian, *i.e.* the bond energies J , and the prefactors to the additional energy terms, such as λ , scale with the temperature T ; *i.e.* if we multiply T by a factor τ , we can multiply the H_0 and the Hamiltonian by the same factor and obtain the same simulation results.

In analogy to the Gamba and Serini PDE model [5,6], we set the diffusion and secretion of the chemoattractant c to:

$$\frac{\partial c}{\partial t} = \alpha \delta_{\sigma_{\mathbf{x}}, 0} - (1 - \delta_{\sigma_{\mathbf{x}}, 0}) \epsilon c + D \nabla^2 c, \quad (3)$$

where $\delta_{\sigma_{\mathbf{x}}, 0} = 1$ inside the cells, α is the rate at which the cells release chemoattractant, and ϵ is the decay rate of the chemoattractant. Thus, every site within the cells secretes the chemoattractant, which decays only in the medium. We solve the PDEs numerically using a finite difference scheme on a lattice matching the CPM lattice, using 20 steps per MCS with $\Delta t = 0.2$. For these parameters the chemoattractant diffuses much more rapidly than the cells, enabling us to ignore the advection that occurs as the cells push the medium forward.

Chemotaxis. We implement preferential motion of the cells along gradients of the chemoattractant c by defining [11]:

$$H' = H - \sum_i \chi \frac{c(\mathbf{x}, \mathbf{t})}{s c(\mathbf{x}, \mathbf{t}) + 1} (1 - \delta_{\sigma_i, \sigma_j}), \quad (4)$$

where χ is the strength of the chemotactic response, and the saturation s sets the Michaelis-Menten constant of the chemotactic response, for which we use $s = 0.01$ by default. For $s = 0$ the cell's response to gradients does not level off at higher concentrations, as in the original method of Savill *et al.* [11], while for large s the cells become unresponsive. Because the chemical field biases cells' boundary copying, each cell moves with an velocity $\mathbf{v} \propto \sqrt{\mu} \sum_j \sum_i P_j(\mathbf{d}_i)$, where the sums run over the sites of the cell and the twenty lattice directions respectively, and $P_j(\mathbf{d}_i)$ denotes the probability that site j copies in lattice direction \mathbf{d}_i . The prefactor $\sqrt{\mu}$ has units of force, but we can also interpret it as the chemotactic strain field [19].

Cell elongation. The HUVEC cells in our cultures elongate progressively as the vessel-like pattern develops. To study how cell elongation affects the pattern, we add a cell-length constraint to the Hamiltonian:

$$H'' = H' + \lambda_L(l - L)^2, \tag{5}$$

where l is the length of the cell along its longest axis, L is its target length, and λ_L is the strength of the length constraint. Larger values of λ_L result in more elongated cells. Following Zajac *et al.* [20], we calculate the short and long axes of the moments of inertia as:

$$\begin{aligned} I_{xx} &= \sum_i (y_i - \bar{y})^2, \\ I_{xy} &= -\sum_i (x_i - \bar{x})(y_i - \bar{y}), \\ I_{yx} &= I_{xy}, \\ I_{yy} &= \sum_i (x_i - \bar{x})^2, \end{aligned} \tag{6}$$

where the sum is over all the sites $\mathbf{x} = (x_i, y_i)$ in the cell. We determine the length l from the largest eigenvalue of I as $l = 2\sqrt{\lambda_b}$, where:

$$\lambda_b = \frac{1}{2}(I_{xx} + I_{yy}) + \frac{1}{2}\sqrt{(I_{xx} - I_{yy})^2 + 4I_{xy}^2}. \tag{7}$$

We can update the inertia tensor locally after each cell extension or retraction, by constructing it from the first and second order moments of the positions of the sites the cells occupy:

$$\begin{aligned} I_{yy} &= \sum_i x_i^2 - \frac{1}{a}(\sum_i x_i)^2, \\ I_{xy} &= -\sum_i x_i y_i - \frac{1}{a}\sum_i x_i \sum_i y_i, \\ I_{xx} &= \sum_i y_i^2 - \frac{1}{a}(\sum_i y_i)^2, \end{aligned} \tag{8}$$

with a the cell area. Thus Eq. [7] determines l without lengthy calculation.

The length constraint can cause cells to split into disconnected patches. We prevent this artifact by introducing a connectivity constraint. To check whether an index copy into site \mathbf{x} will change local connectivity, we count how many of its neighbors \mathbf{x}'_i have equal index to \mathbf{x} while the next in cyclic order has unequal spin. If this quantity $\sum_i \delta_{\sigma(\mathbf{x}), \sigma(\mathbf{x}'_i)} (1 - \delta_{\sigma(\mathbf{x}), \sigma(\mathbf{x}'_{i+1})}) > 2$, with the sum running in cyclic order, changing the site will destroy the local connectivity. We have currently only implemented this algorithm for second-order neighborhoods (*i.e.* 8 neighbours). This test for connectivity loss gives “false positives” for non-convex patches, which occur in our simulations when cells suddenly shrink, for example during “apoptosis” [18]. Instead of introducing a very expensive ($O(N^2)$) global connectivity test, we tolerate temporary violations of connectivity for large energy drops. The bond energies ensure that the lifetime of disconnected patches is short. We assume that cell fragmentation is energetically costly, and set a high energy threshold H_0 (typically $H_0 = 500$) *iff* the attempted update would change the local connectivity.

2.2 Simulation Set-Up and Initialization

In our partial differential equations (PDE), we set boundary values to zero (*i.e.* the boundaries absorb the chemoattractant), while for the CPM we implement repellent boundary conditions by setting the cell-boundary binding energy to $J_{CB} = 100$. We use a 500×500 lattice, where each lattice site represents an area of about $4\mu m^2$. Cells have actual areas of around 45 lattice sites, equivalent to a typical endothelial cell area of around $150\mu m^2$ [21]. To diminish boundary effects we initially disperse n cells randomly within a centered 333×333 square. For $n \geq 3000$ we disperse the cells all over the field to minimize cell overlap. After each Monte Carlo Step (MCS) we update the PDE 20 times with $\Delta t = 0.2$.

2.3 Morphometry

We characterize the patterns by measuring the average size \bar{L}_a of the open spaces which the vessel-like structures enclose (*lacunae*). $\bar{L}_a = 1/N \sum_i L_{a_i}$, with N the number of lacunae and L_{a_i} the size of each lacuna, which we identify using a standard connected-component labeling algorithm [1].

3 Results

Figs. 2 and 3 review our results. Fig. 2a reproduces the results of the Gamba and Serini PDE model [5,6] in our cell-oriented model. The cell-adhesion settings are strongly adhesive ($\gamma_{cM} = 17.5$). The cells aggregate into cords and nodes, typical of HUVEC Matrigel cultures (Fig. 1) and the Gamba-Serini model. As the cell density increases, we find a percolation transition as in the Gamba-Serini model [5]; for low densities, $n < 1000$, the cells do not form a connected network, while for high densities, $n > 1000$, all cells interconnect (see Fig. 2a).

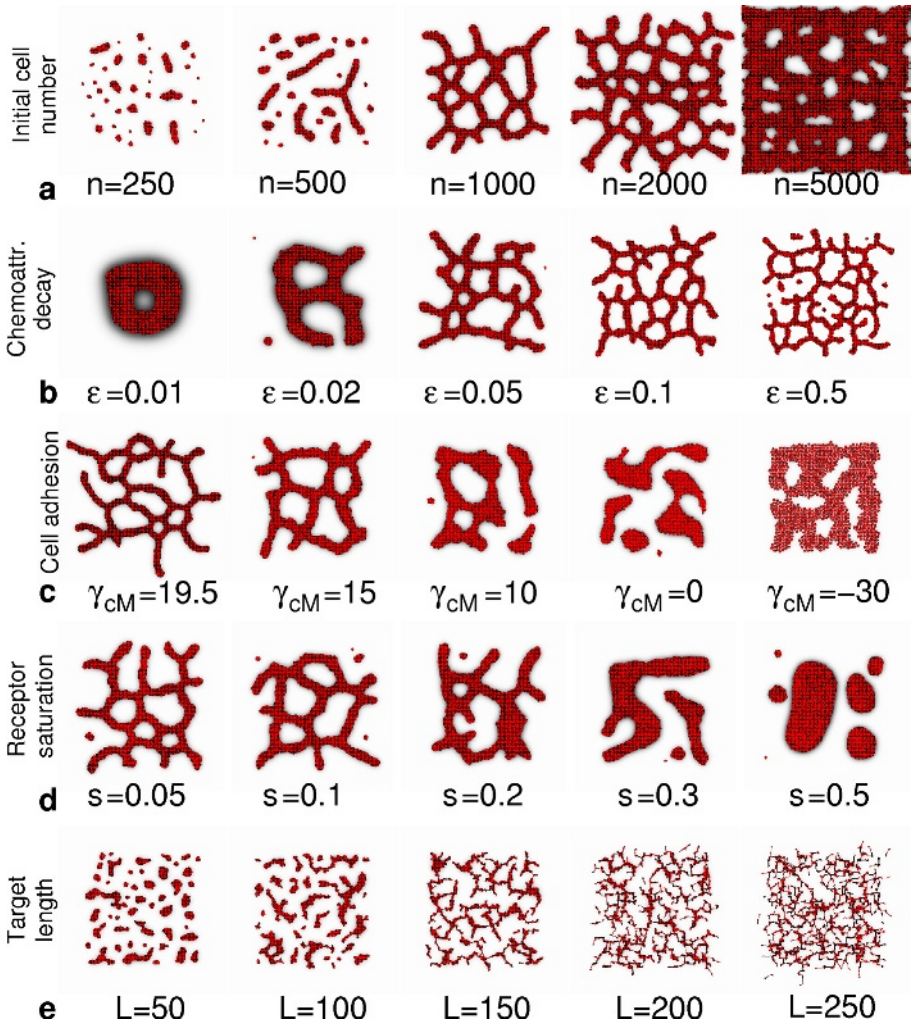


Fig. 2. Overview of parameter sweeps. Typical cell patterns after 5000 MCS. Lattice size 500×500 , $n = 1000$ scattered within inner 333×333 subfield (e: $n = 555$). Parameters were $T = 50$, $\lambda_A = 50$, $A = 50$, $\gamma_{cM} = 17.5$, $s = 0.01$, $\chi = 2000$, $\alpha = 0.01$, $\epsilon = 0.05$, $D = 1$, $\lambda_L = 0$ (e: $\lambda_L = 1.0$), unless indicated otherwise.

Also, as in the Gamba-Serini model, the size of the lacunae depends on the rate of chemoattractant decay, as Fig. 2b shows.

In Figs. 2c-e, we systematically modify the Gamba-Serini model by changing the biophysical properties of the individual cells. First, we study the role of intercellular adhesion. In our model, cell adhesion is essential. If we reduce the adhesivity of the endothelial cells, a network no longer forms and the cells aggregate into “islands” (Fig. 2c). Like the Gamba-Serini model, our model can

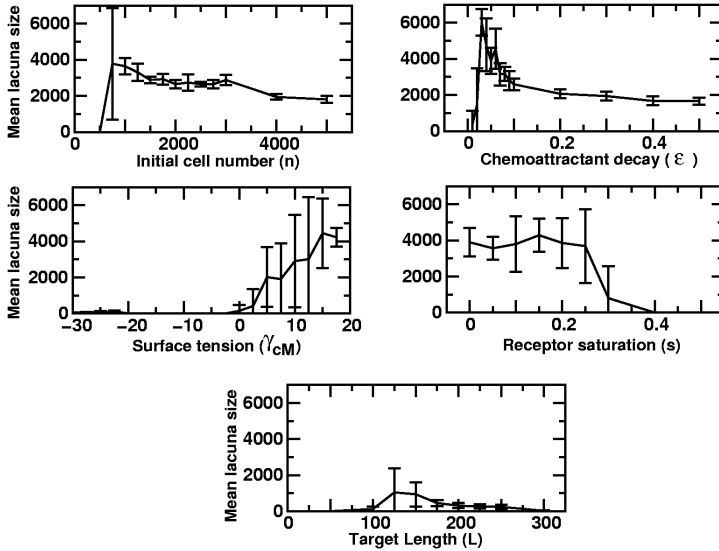


Fig. 3. Dependence of lacuna size on model parameters, after 5000 Monte Carlo steps. Parameters as in Fig. 2. Error bars indicate standard deviations ($n = 5$)

also form networks without cell adhesion, but these networks are unstable and decay into an “island-like” pattern (results not shown).

Fig. 2d shows the effect of changes in s , the threshold for chemotaxis saturation (sensitivity) (see eq. 4). Up to around $s = 0.1$ vessel-like patterns form, while for larger values more amorphous patterns with larger clusters and few lacunae form. The lacuna size becomes more variable for larger values of s (see Fig. 3d).

In the *in vitro* culture experiments, the endothelial cells elongate during vessel-like patterning. Although elongation is not necessary for vessel-like patterning in our model, cell elongation is one of the first observable signs of vessel-like patterning in HUVEC cultures. In Fig. 2e and Fig. 3e we investigate the effect of cell elongation on patterning at low cell densities ($n = 555$). Cell elongation facilitates the interconnection of isolated parts of the pattern (see Fig. 3e). For very large length constraints ($L > 300$) the cells fragment, after which the vessel-like pattern no longer interconnects. At higher densities, when the pattern already fully interconnects even for round cells, cell elongation has no effect on lacuna size, but affects the shape of the lacunae (results not shown).

4 Discussion and Conclusions

Computational screening of the parameter dependence of patterning may help to direct experiments to identify the key regulators of vascular development and suggest new hypotheses. If chemotaxis drives vascular development, as in the

Gamba-Serini model, our simulations suggest that endothelial cell adhesion is essential to form stable vascular networks. Furthermore, our simulations suggest that pattern formation changes qualitatively when the receptors saturate at lower concentrations of chemoattractant. We could test this effect experimentally by specifically inhibiting the production of receptors, in which case the remaining receptors would saturate at lower concentrations, or by adding receptors with higher affinity. Cell extension also strongly affects the multicellular pattern, reducing the cell density network formation requires. Biological experiments might attempt to specifically target the elongation of the endothelial cells. Preliminary results also show that cell motility above a minimum required velocity does not significantly affect patterning (not shown). Continuous models have great difficulty assessing the role of these parameters, in particular of intercellular adhesion and cell morphology.

In our ongoing work we are refining and validating our computational model by obtaining experimentally derived values for the model parameters and by comparing our simulation results quantitatively to time-lapse videomicroscopy experiments. We are analyzing the dynamics of patterning in HUVEC cultures under different physiological and pathological conditions and comparing these to the computational model's dynamics for similar simulated conditions. Gradual cell elongation, rather than the instantaneous elongation that we employed here, may change the model's dynamics. We also plan to model the interaction of the individual cells with the viscoelastic extracellular matrix, which experiments and theory [4] suggest is crucial to *in vitro* vasculogenesis. These studies may lead to better understanding of the biophysical mechanisms of vascular development, which will suggest new experimental tests of the genetic and biophysical regulation of vascular development.

Acknowledgments. This material is based upon work supported by the National Science Foundation under Grants MRI-0116050 and IBN-0083653, a Pervasive Technologies Laboratories Fellowship (Indiana University Bloomington), an IBM Innovation Institute Award and NASA NAG 2-1619, the Indiana University Biocomplexity Institute, and the Indiana University AVIDD program. We thank Dr. Sergey Brodsky and Prof. Michael Goligorsky of the Dept. of Medicine at New York Medical College for help with Fig. 1. R.M. developed parts of the simulation software during work with Prof. Paulien Hogeweg at Utrecht University, The Netherlands.

References

1. Dougherty, E.R., Lotufo, R.A.: Hands-on Morphological Image Processing. Volume TT59 of Tutorial Texts in Optical Engin. SPIE Press, Bellingham, WA, USA (2003)
2. Segura, I., Serrano, A., De Buitrago, G.G., Gonzalez, M.A., Abad, J.L., Claveria, C., Gomez, L., Bernad, A., Martinez-A, C., Riese, H.H.: Inhibition of programmed cell death impairs *in vitro* vascular-like structure formation and reduces *in vivo* angiogenesis. *FASEB J.* **16** (2002) 833–841

3. Chen, J., Brodsky, S., Li, H., Hampel, D.J., Miyata, T., Weinstein, T., Gafter, U., Norman, J.T., Fine, L.G., Goligorsky, M.S.: Delayed branching of endothelial capillary-like cords in glycated collagen I is mediated by early induction of PAI-1. *Am. J. Physiol.-Renal* **281** (2001) F71–F80
4. Namy, P., Ohayon, J., Tracqui, P.: Critical conditions for pattern formation and in vitro tubulogenesis driven by cellular traction fields. *J. Theor. Biol.* **227** (2004) 103–120
5. Gamba, A., Ambrosi, D., Coniglio, A., De Candia, A., Di Talia, S., Giraudo, E., Serini, G., Preziosi, L., Bussolino, F.: Percolation morphogenesis and burgers dynamics in blood vessels formation. *Phys. Rev. Lett.* **90** (2003) 118101
6. Serini, G., Ambrosi, D., Giraudo, E., Gamba, A., Preziosi, L., Bussolino, F.: Modeling the early stages of vascular network assembly. *EMBO J.* **22** (2003) 1771–1779
7. Manoussaki, D., Lubkin, S.R., Vernon, R.B., Murray, J.D.: A mechanical model for the formation of vascular networks in vitro. *Acta Biotheor.* **44** (1996) 271–282
8. Manoussaki, D.: A mechanochemical model of angiogenesis and vasculogenesis. *ESAIM-Math. Model. Num.* **37** (2003) 581–599
9. Takahashi, K., Ishikawa, N., Sadamoto, Y., Sasamoto, H., Ohta, S., Shiozawa, A., Miyoshi, F., Naito, Y., Nakayama, Y., Tomita, M.: E-cell 2: Multi-platform e-cell simulation system. *Bioinformatics* **19** (2003) 1727–1729
10. Silicon cell project. (<http://www.siliconcell.net>)
11. Savill, N.J., Hogeweg, P.: Modelling morphogenesis: from single cells to crawling slugs. *J. Theor. Biol.* **184** (1997) 229–235
12. Marée, A.F.M., Hogeweg, P.: How amoeboids self-organize into a fruiting body: Multicellular coordination in *Dictyostelium discoideum*. *P. Natl. Acad. Sci. USA* **98** (2001) 3879–3883
13. Zajac, M., Jones, G.L., Glazier, J.A.: Model of convergent extension in animal morphogenesis. *Phys. Rev. Lett.* **85** (2000) 2022–2025
14. Turner, S., Sherratt, J.A.: Intercellular adhesion and cancer invasion: a discrete simulation using the extended Potts model. *J. Theor. Biol.* **216** (2002) 85–100
15. Kiskowski, M.A., Alber, M.S., Thomas, G.L., Glazier, J.A., Bronstein, N.B., Pu, J., Newman, S.A.: Interplay between activator-inhibitor coupling and cell-matrix adhesion in a cellular automaton model for chondrogenic patterning. *Dev. Biol.* **271** (2004) 372–387
16. Glazier, J.A., Graner, F.: Simulation of the differential adhesion driven rearrangement of biological cells. *Phys. Rev. E* **47** (1993) 2128–2154
17. Izaguirre, J.A., Chaturvedi, R., Huang, C., Cickovski, T., Coffland, J., Thomas, G., Forgacs, G., Alber, M., Hentschel, G., Newman, S.A., Glazier, J.A.: COMPUCELL, a multi-model framework for simulation of morphogenesis. *Bioinformatics* **20** (2004) 1129–1137
18. Hogeweg, P.: Evolving mechanisms of morphogenesis: on the interplay between differential adhesion and cell differentiation. *J. Theor. Biol.* **203** (2000) 317–333
19. Jiang, Y., Swart, P.J., Saxena, A., Asipauskas, M., Glazier, J.A.: Hysteresis and avalanches in two-dimensional foam rheology simulations. *Phys. Rev. E* **59** (1999) 5819–5832
20. Zajac, M., Jones, G.L., Glazier, J.A.: Simulating convergent extension by way of anisotropic differential adhesion. *J. Theor. Biol.* **222** (2003) 247–259
21. LaRue, A.C., Mironov, V.A., Argraves, W.S., Czirók, A., Fleming, P.A., Drake, C.J.: Patterning of embryonic blood vessels. *Dev. Dynam.* **228** (2003) 21–29